NJC

PAPER

View Article Online
View Journal | View Issue

Cite this: *New J. Chem.*, 2018, 42, 483

Synergistic effects of Zn and Pd species in TiO_2 towards efficient photo-reduction of CO_2 into CH_4†

Yanlong Yu,‡[a] Zijian Lan,‡[a] Limei Guo,[a] Enjun Wang,[b] Jianghong Yao*[a] and Yaan Cao *[a]

Received 1st September 2017,
Accepted 26th November 2017

DOI: 10.1039/c7nj03305b

rsc.li/njc

A Zn and Pd co-modified TiO_2 photocatalyst exhibits remarkably enhanced photocatalytic activity upon reduction of CO_2 into CH_4. Owing to the synergistic effect of unique O–Zn–Cl and O–Pd–O species, TiO_2–PdX–ZnY presents enhanced visible absorption and efficient charge carrier separation. It can be deduced from theoretical calculations and experimental results that the energy levels of O–Zn–Cl and O–Pd–O satisfy the redox potential of CO_2 reduction, improving the photocatalytic performance. These results suggest that introducing multi-surface species to produce synergetic effects is a feasible route for efficient photocatalysis.

Introduction

Photo-reduction of CO_2 into CH_4 *via* semiconductor photocatalysis has been investigated by many researchers since it uses solar light to convert CO_2 into a valuable carbon fuel, methane.[1–5] The mechanism of photo-reduction of CO_2 into CH_4 is explained as follows:[6–13]

$$\text{Catalyst} + h\nu \rightarrow e^- + h^+$$

$$H_2O + h^+ \rightarrow {}^\bullet OH + H^+ \quad (1)$$

$${}^\bullet OH + H_2O + 3h^+ \rightarrow O_2 + 3H^+$$

$$2H_2O + 4h^+ \rightarrow O_2 + 4H^+ \; E^0_{redox} = 0.82 \text{ V } \textit{vs.} \text{ NHE} \quad (2)$$

$$2CO_2 + 4e^- \rightarrow 2CO + O_2 \; E^0_{redox} = -0.12 \text{ V } \textit{vs.} \text{ NHE}$$

$$2CO + 4e^- \rightarrow 2{}^\bullet C + O_2$$

$${}^\bullet C + 4e^- + 4H^+ \rightarrow CH_4 \; E^0_{redox} = 0.13 \text{ V } \textit{vs.} \text{ NHE}$$

$$CO_2 + 8e^- + 8H^+ \rightarrow CH_4 + 2H_2O \; E^0_{redox} = -0.24 \text{ V } \textit{vs.} \text{ NHE} \quad (3)$$

Electrons and holes are excited under proper irradiation (eqn (1)). These charge carriers would further react with surface adsorbed CO_2 and H_2O molecules to generate CO and carbon radicals ($^\bullet$C), which would further react with H^+ to produce the final product, CH_4 (eqn (2) and (3)). Furthermore, it is considered as necessary for highly active catalysts that the position of the conduction band and the valence band should satisfy the redox potential discussed above.

TiO_2 is one of the most promising photocatalysts for the photoreduction of CO_2 into CH_4, due to its good performance and stability.[2,6,8,14–18] However, the catalytic application of TiO_2 is still limited because of its large band-gap, its rapid recombination of charge carriers, and especially the mismatch of its redox potential for the photoreduction of CO_2 into CH_4. Its modification with metal or nonmetal elements is considered as an effective method to enhance its visible response and separate the charge carriers as well as design and adjust the energy level of the photocatalyst, leading to full use of the photogenerated charge carriers. It is found that introducing Zn or Mn ions into the TiO_2 system would create new doping energy levels below the conduction band, extending the response into the visible region and separating the charge carriers.[19,20] Moreover, it is also noted that introducing Cu, C and Pd species into the TiO_2 system would enhance the visible response and generate more charge carriers by forming new energy levels above the valence band.[19,21]

TiO_2 doped or modified with Pd[22–27] has been investigated to improve the photocatalytic performance recently. Electrons and holes would transfer to the surface to participate in the photo-reduction reaction more easily and rapidly *via* these doping energy levels. In our previous work, it was found that

[a] *MOE Key Laboratory of Weak-Light Nonlinear Photonics, Ministry of Education, TEDA Applied Physics Institute and School of Physics, Nankai University, Tianjin 300457, China. E-mail: yaojh@nankai.edu.cn, caoya@nankai.edu.cn*
[b] *Hefei Institutes of Physical Science, Chinese Academy of Sciences, Hefei 230031, China*

† Electronic supplementary information (ESI) available. See DOI: 10.1039/c7nj03305b
‡ Both authors contributed equally.

co-modified TiO_2 with Pd and other elements could show a strong visible response and separate charge carriers efficiently,[28–30] exhibiting remarkable catalytic performance. Moreover, the existence of unique Zn species on the TiO_2 surface is also confirmed.[23]

To date, for TiO_2 co-modified with Pd and other elements the band structure, its relationship with the redox potential for the reduction of CO_2 into CH_4, and the behaviour of the photogenerated charge carriers are still not investigated. Furthermore, the synergistic effect of Pd with other elements and their relationships with the visible response, separation of charge carriers and redox ability as well as the photocatalytic activity of the photocatalyst still need further investigation. And the photocatalytic mechanism should be discussed in detail.

In this work, Pd and Zn co-modified TiO_2 exhibited remarkable photocatalytic activity. This paper focuses on the synergistic effect of Pd and Zn species on the surface and their influence on the band structure, visible response, separation of the photogenerated charge carriers and photo-catalytic activity in detail. The photocatalytic mechanism is also investigated for the reduction of CO_2 into CH_4.

Experimental

Synthesis of TiO_2–PdX–ZnY

All chemicals used in this work were of analytical grade. At room temperature, different amounts of $PdCl_2$ solution, $Zn(NO_3)_2$ and 1 mL of HCl solution (12 mol L^{-1}) were dissolved in 40 mL of ethanol. Under violent stirring for 30 min, 12 mL of $Ti(OC_4H_9)_4$ and 1 mL of deionized water were added dropwise (pH = 0.5). The mixed solution was stirred until TiO_2 gel is formed. After 24 hours of aging, the TiO_2 gel was heated at 373 K for 10 h and calcined at 723 K for 2.5 h. These synthesized samples are denoted as TiO_2–PdX–ZnY (X = 1.5–3%; Y = 3–7%), where X and Y stand for the nominal molar ratio of Zn^{2+} and Pd^{2+} to Ti^{4+} (Zn/Ti and Pd/Ti), respectively. Pure TiO_2, 5% Zn modified TiO_2 (TiO_2–Zn) and 1.5% Pd modified TiO_2 (TiO_2–Pd) were synthesized by the same process just without $PdCl_2$ and/or $Zn_2(NO_3)_2$.

Characterizations

The Raman spectrum was acquired on a Renishaw in *Via* Raman microscope with the 785 nm line of a Renishaw HPNIR 785 semiconductor laser. The BET surface areas were obtained by measuring nitrogen adsorption–desorption isotherms at 77 K (Micromeritics Automatic Surface Area Analyzer Gemini 2360, Shimadzu), after degassing at 453 K. XPS was performed with an ESCA Lab 220i-XL spectrometer by using an unmonochromated Al Ka X-ray source (148.6 eV). All spectra have been calibrated using the adventitious C1s peak at 284.8 eV. Diffuse reflectance UV-vis absorption spectra (UV-vis DRS) were obtained using a UV-vis spectrometer (U-4100, Hitachi). Photoluminescence (PL) spectra were measured on a spectrometer (Spex 1702), a photomultiplier tube (PMT, Hamamatsu R943), a lock-in amplifier, and a computer for data processing using the 325 nm line of a nano-second Nd:YAG laser (NL303G) as the excitation source. Surface photovoltage spectra (SPS) were acquired on a solid-junction photovoltaic cell of ITO/sample/ITO equipped with a lock-in amplifier (Model SR830, DSP) and synchronized with a light chopper. Monochromatic light was obtained by passing light from a 500 W xenon lamp (CHF-XQ 500W) through a double prism monochromator (WDG30-2).

Photo-reduction of CO_2

The photoreduction of CO_2 into CH_4 is used to estimate the performance of the photocatalyst. A 500 W spherical Xenon arc lamp (Philips, Belgium, 35 mW cm^{-2}, 290–800 nm) was applied as the light source in this experiment. There was one glass sheet (9.4 cm^2) placed at the bottom of the sealed reaction vessel (410 mL). About 150 mg of the as-prepared samples was tiled on the glass. The light beam was vertical to the glass and the lamp was 10 cm away from the surface of the glass. The reaction vessel was filled with CO_2 gas (99.99%) for 45 min before it was sealed. Then the reaction mixture was injected with 2 mL of water. About 0.4 mL of the gas in this vessel was extracted every 120 min. A gas chromatograph (Techcomp GC-7890F, equipped with a 1 m × 3 mm TDX-01 packed column and a flame ionization detector (FID)) was used to detect the concentration of the produced CH_4 and CO. The relative humidity and temperature in the reactor during the photosynthesis process were maintained as 80% and 30 °C.

Results and discussion

The photo-reduction of CO_2 into CH_4 under Xe lamp irradiation is applied to estimate the catalytic performance of the obtained TiO_2-based photocatalysts, as shown in Fig. 1, and Table 1. CO is the intermediate product (Fig. S1 and Table S1, ESI†) and CH_4 is the final product. There is no other gas product detected, such as H_2 and CH_3OH. After 8 h of irradiation, only 0.350 μmol of CH_4 is detected for pure TiO_2. TiO_2–Zn exhibited a finite photocatalytic activity and 0.851 μmol of CH_4 was generated. The photocatalytic performance of TiO_2–Pd was enhanced effectively and 3.59 μmol of CH_4 was generated. After the introduction of Zn and Pd into TiO_2, the TiO_2–PdX–ZnY (X = 1.5–3%; Y = 3–7%) samples exhibited remarkably enhanced photocatalytic activity. Furthermore, the TiO_2–Pd1.5%–Zn5% sample represented the highest catalytic performance of all photocatalysts and about 7.99 μmol of CH_4 was detected, which is almost twice that for TiO_2–Pd and twenty times higher than that for pure TiO_2. The results indicated that the photocatalytic activity for the Zn and Pd co-modified TiO_2 photocatalyst was enhanced remarkably due to the introduction of both Zn and Pd into TiO_2. In addition, it was found from XPS that the amount of C before and after the photocatalytic reaction was 15.34% and 18.63%, respectively, suggesting that the surface absorbed carbon in the photocatalyst did not react with CO_2 to generate CO.

The structure and the existing states of Pd and Zn were investigated by the Raman, XRD and XPS spectra for TiO_2, TiO_2–Zn, TiO_2–Pd and TiO_2–PdX–ZnY samples. For the Raman spectra (Fig. 2 and Fig. S2, ESI†), all samples showed typical

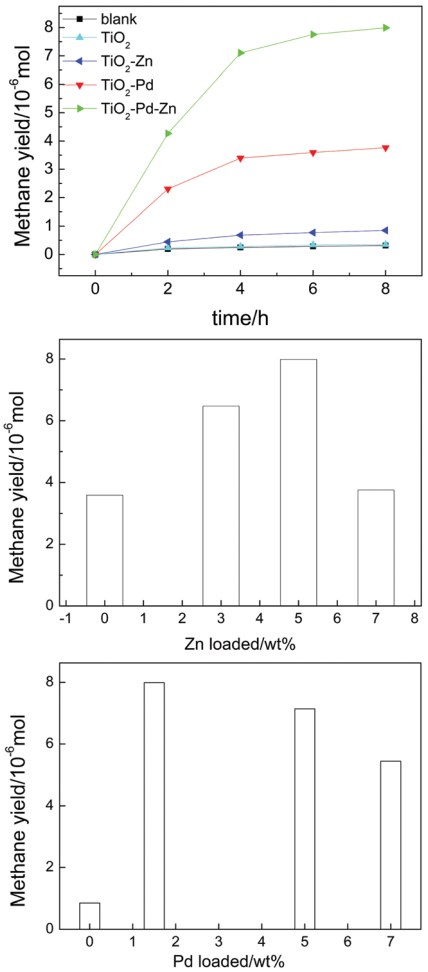

Fig. 1 Amount of CH_4 generation for TiO_2, TiO_2–Pd, TiO_2–Zn and TiO_2–Pd1.5%–Zn5% (a), TiO_2–Pd1.5%–ZnY% (b) and TiO_2–PdX–Zn5% (c) under Xe lamp irradiation after 8 h.

Table 1 Photocatalytic activity of pure TiO_2, TiO_2–Zn, TiO_2–Pd and TiO_2–PdX–ZnY (X = 1.5–3%; Y = 3–7%) samples under Xe lamp irradiation after 8 h

Sample	CH_4 (10^{-6} mol)	Specific photocatalytic activity (10^{-6} mol g^{-1} h^{-1})[b]
Blank[a]	0.31 ± 0.01	—
TiO_2(P25)	0.36 ± 0.02	0.30 ± 0.02
TiO_2	0.35 ± 0.03	0.29 ± 0.02
TiO_2–Zn	0.85 ± 0.02	0.71 ± 0.02
TiO_2–Pd	3.77 ± 0.47	3.14 ± 0.39
TiO_2–Pd1.5%–Zn3%	6.48 ± 0.27	5.40 ± 0.23
TiO_2–Pd1.5%–Zn5%	7.99 ± 0.28	6.66 ± 0.23
TiO_2–Pd1.5%–Zn7%	3.60 ± 0.35	3.00 ± 0.29
TiO_2–Pd5%–Zn5%	7.14 ± 0.45	5.95 ± 0.38
TiO_2–Pd7%–Zn5%	5.44 ± 0.73	4.53 ± 0.61

[a] Blank is the photolysis of CO_2. [b] Specific photocatalytic activity of CH_4, CH_4 generation amount per hour per unit mass of the catalyst. The experimental error in the photocatalytic results is <5% based on triplicate runs.

characteristic bands and the vibrational modes of anatase.[31] In addition, for TiO_2–Zn as well as TiO_2–PdX–ZnY samples (Fig. S2, ESI†), two additional weak Raman peaks around 256 cm^{-1} and 333 cm^{-1} were observed, ascribed to the stretching

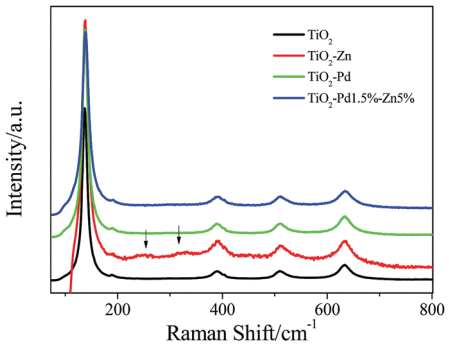

Fig. 2 Raman spectra of TiO_2, TiO_2–Zn, TiO_2–Pd and TiO_2–Pd1.5%–Zn5%.

modes of Zn–Cl and Zn–O bonds, respectively.[20] XRD results for all samples (Fig. S3 and Table S2, ESI†) also confirm that only anatase exists for these samples, which is in good agreement with the Raman spectrum mentioned above. Furthermore, after the introduction of Pd and Zn, the specific surface areas (BET) increase in the order of TiO_2 < TiO_2–Zn < TiO_2–Pd < TiO_2–Pd–Zn. The crystallite sizes decrease in the order of TiO_2–Pd–Zn < TiO_2–Zn < TiO_2–Pd < TiO_2. The detailed existing states of Zn and Pd are investigated by XPS.

Fig. 3 shows the XPS spectra of TiO_2, TiO_2–Pd, TiO_2–Zn and TiO_2–Pd1.5%–Zn5%. For the Pd 3d spectra (Fig. 3A), the peaks of Pd $3d_{5/2}$ for TiO_2–Pd and TiO_2–Pd1.5%–Zn5% locate at about 336.7 eV, attributed to the O–Pd–O structure on the TiO_2 surface (one Pd^{2+} ion linked with two unsaturated O^{2-} ions).[19,32] For XPS Cl 2p spectra (Fig. 3B), the peak centered at about 198.1 eV for TiO_2 and TiO_2–Pd is ascribed to Cl 2p of the O–Ti–Cl species on the TiO_2 surface. For the TiO_2–Zn and TiO_2–Pd1.5%–Zn5% samples, the peaks centered at about 198.9 eV and 198.7 eV respectively, are between those of $TiCl_4$ (198.2 eV) and $ZnCl_2$ (199.7 eV).[9] Furthermore, as shown in Fig. 3C, the center of the Zn $2p_{3/2}$ peak for the Zn 2p spectra of TiO_2–Zn (1022.1 eV) and TiO_2–Pd–Zn (1022.0 eV) locates between those of ZnO (1021.5 eV)[33] and $ZnCl_2$ (1022.5 eV).[34] This indicates that one Zn^{2+} ion links with one unsaturated O atom and one Cl^- ion to exist as O–Zn–Cl species.[20,34] Moreover, compared with TiO_2 (2.01%) and TiO_2–Pd (2.36%), the atom percentage calculated from the XPS also increases remarkably for TiO_2–Zn (6.49%) and TiO_2–Pd–Zn (5.25%). Hence, it is concluded that unique O–Pd–O and O–Zn–Cl species are formed on the surface of TiO_2.

To determine the band structure of TiO_2–PdX–ZnY, the valence bands of XPS spectra and absorption spectra are shown in Fig. 4. For the XPS valence band spectra (Fig. 4A), the energy levels in all samples are aligned by the Fermi level of the XPS instrument (4.1 eV).[35] The BE of the onset edge for O 2p revealed the gap between the valence band top and the Fermi level (E_f). The onset edge of the valence band top for TiO_2 is at about +2.7 eV (+2.3 V, *vs.* NHE). The onset edge for TiO_2–Zn almost remains unchanged compared with TiO_2, implying that the energy level of O–Zn–Cl species is far from the valence band of TiO_2. It is found from the theoretical calculation (Fig. S4, ESI†) that a new energy level corresponding to O–Zn–Cl species

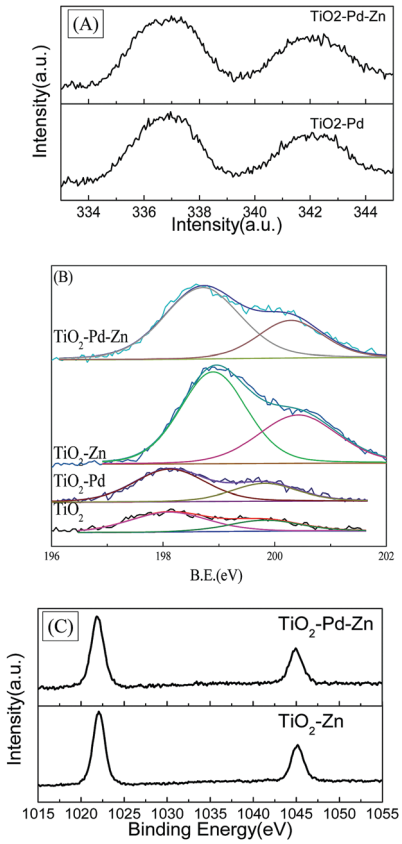

Fig. 3 (A) XPS Pd 3d spectra of TiO_2–Pd and TiO_2–Pd1.5%–Zn5%; (B) Cl 2p spectra of TiO_2, TiO_2–Pd, TiO_2–Zn and TiO_2–Pd–Zn; (C) Zn 2p of TiO_2–Pd and TiO_2–Pd1.5%–Zn5%.

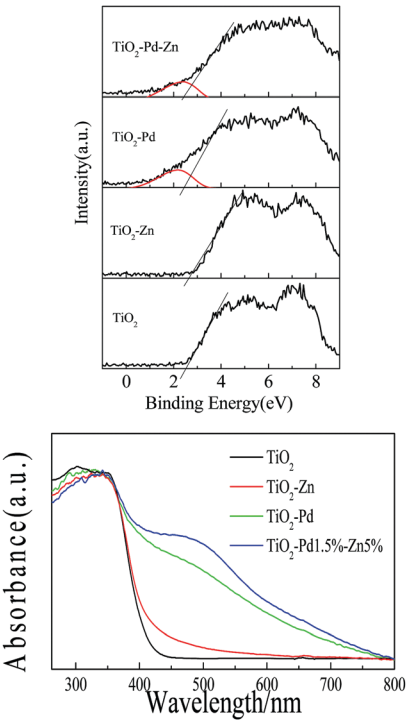

Fig. 4 (A) XPS valence band spectra, and (B) absorption spectra of TiO_2, TiO_2–Zn, TiO_2–Pd and TiO_2–Pd1.5%–Zn5%.

occurred below the conduction band of TiO_2, which mainly consists of Zn 4s and Cl 3p orbitals. Moreover, for TiO_2–Pd and TiO_2–Pd–Zn, a small hump of about +2.1 eV (+1.7 eV, *vs.* NHE) is caused by the introduced Pd 4d orbital corresponding to the O–Pd–O species, whose energy level can be estimated to be at 0.6 eV above the valence band of TiO_2. The theoretical simulation (Fig. S4, ESI†) also confirmed that new energy levels, composed of the Pd 4d orbital and hybridized with O 2p and Ti 3d states, occurred above the valence band of TiO_2 for TiO_2–Pd.

The absorption spectra of all samples are plotted in Fig. 4B. TiO_2 shows strong absorption in the UV region caused by the band-to-band transition. The band gap for TiO_2 is estimated to be 3.1 eV, as the onset edge is at about 400 nm. Weak absorption centered at about 450 nm from 400 nm to 600 nm for TiO_2–Zn is observable. Electrons in the valence band can be excited to the energy level of O–Zn–Cl species next to the conduction band. The stronger visible response is observed for TiO_2–Pd, as the electrons from O–Pd–O species can be excited to the conduction band of TiO_2. Moreover, as we expect, owing to the synergistic effect of O–Pd–O and O–Zn–Cl species, TiO_2–PdX–ZnY represents the strongest absorption in the visible region (Fig. 4B and Fig. S3, ESI†), and the absorption can be further improved by increasing the amount of Pd and Zn. These results indicate that introducing Zn into the TiO_2–Pd system could lead to the synergetic effect of Pd and Zn, which may enhance the visible response, and match the band structure with the redox potential of photo-reduction of CO_2 into CH_4, resulting in enhanced catalytic activity.

To investigate the behaviour of charge carriers, photoluminescence spectra (PL), time resolved PL and surface photovoltaic spectra (SPS) were acquired, as shown in Fig. 5 and 6 and Table 2. For the photocatalyst, the electrons fell into the oxygen

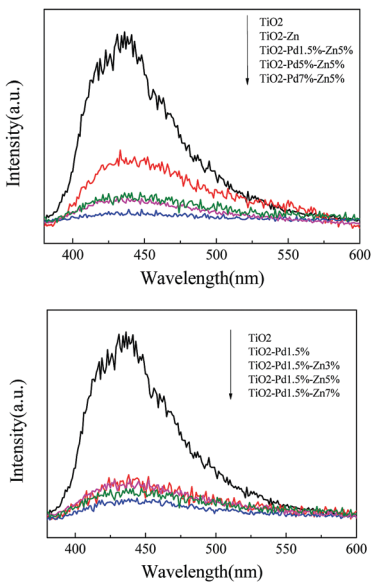

Fig. 5 Photoluminescence spectra (PL) of TiO_2, TiO_2–Zn, TiO_2–Pd, and TiO_2–PdX–Zn5% (A) and TiO_2–Pd1.5%–ZnY (B).

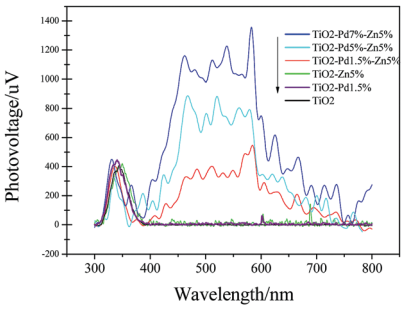

Fig. 6 Surface photovoltaic spectra (SPS) of TiO_2, TiO_2–Zn, TiO_2–Pd and TiO_2–PdX–ZnY.

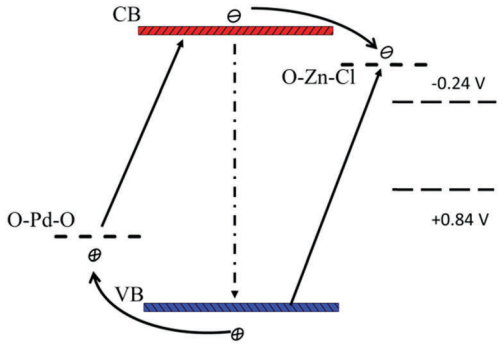

Fig. 7 Schematic band structure of TiO_2–PdX–ZnY as well as the photocatalytic mechanism (not drawn to scale).

Table 2 Time constant τ_1 and τ_2 through double exponential decay fitting for TiO_2, TiO_2–Zn, TiO_2–Pd, and TiO_2–Pd1.5%–Zn5%

	TiO_2	TiO_2–Zn	TiO_2–Pd	TiO_2–Pd1.5%–Zn5%
τ_1 (ns)	0.295	0.298	0.294	0.291
τ_2 (ns)	3.059	3.876	4.038	4.382

vacancies from the conduction band through a nonirradiative process (τ_1) and recombined with holes *via* an irradiative process (τ_2), resulting in fluorescence emission. Hence, quenching of the PL intensity and prolonged life-time of charge carriers indicate efficient suppression of the recombination for charge carriers. Fig. 5 shows the PL spectra of TiO_2, TiO_2–Zn, TiO_2–Pd and TiO_2–PdX–ZnY. It is observed from Fig. 5A that the emission intensity of TiO_2–Zn is weakened compared with TiO_2, owing to the surface energy level of O–Zn–Cl species. For TiO_2–Pd (Fig. 5B), the PL intensity is quenched significantly because the holes transfer from the valence band to the O–Pd–O species. And the PL emission for TiO_2–PdX–ZnY is further quenched with the increase of Zn or Pd owing to the contribution from both the Zn and Pd species (Fig. 5A and B). Moreover, the τ_1 and τ_2 values related to the nonirradiative and irradiative processes are shown in Table 2. The τ_2 values for TiO_2–Zn and TiO_2–Pd are greater than that for TiO_2, as the electrons could transfer from the conduction band of TiO_2 to the levels of O–Zn–Cl species or the holes could move from the valence band to the energy levels of O–Pd–O species. The τ_2 values for TiO_2–Pd1.5%–Zn5% samples are greater than those of TiO_2–Zn and TiO_2–Pd due to the synergistic effect of Pd and Zn species. These results suggest that the photo-generated electrons and holes were separated more efficiently for Zn and Pd co-modified TiO_2 samples than TiO_2–Zn and TiO_2–Pd.

As shown in Fig. 6, SPS reveals the separation behaviours of photogenerated charge carriers. The higher light response (peak intensity) usually indicates that more charge carriers are separated. For all samples, the response peaks around 350 nm are caused by band–band transition. TiO_2 shows no SPS response in the visible region (400 nm to 800 nm). And TiO_2–Zn and TiO_2–Pd exhibit poor SPS response in the visible region compared with TiO_2. This indicates that the photo-generated charge carriers were not separated efficiently from the surface of the catalyst under visible irradiation, when only Zn or Pd species were introduced into the TiO_2 system. Moreover, the TiO_2–PdX–ZnY samples exhibited a significant light response in the visible region compared to the others. With increasing Pd content, the light response of TiO_2–PdX–Zn5% is further enhanced, which may be attributed to the synergistic effect of O–Zn–Cl and O–Pd–O species. This suggests that more electrons and holes were generated and separated for the TiO_2–PdX–ZnY samples than the TiO_2–Pd or TiO_2–Zn samples, respectively.

According to the SPS results (Fig. 6), the synergistic effect of Pd and Zn species on the surface can be analyzed by the schematic band structure of TiO_2–PdX–ZnY samples (Fig. 7). TiO_2 shows no visible response and the recombination rates of holes and electrons are quite high. For TiO_2–Zn, the weaker SPS response in the visible region is assigned to the limited visible absorption in the visible region. Stronger visible absorption is observed for TiO_2–Pd, caused by the O–Pd–O species. Moreover, the SPS response in the visible region is poor, due to the rapid recombination of charge carriers, as shown in Fig. 7. For TiO_2–PdX–ZnY, the higher SPS light response in the visible region indicates the more efficient generation and separation of photogenerated charge carriers, owing to the synergistic effect of Pd and Zn species on the TiO_2 surface. Electrons were generated from the valence band to the energy level of Zn species. Furthermore, the electrons in the conduction band arising from Pd species can also transfer to the levels of O–Zn–Cl species, instead of recombining with holes in the valence band, separating photogenerated charge carriers efficiently. Therefore, for TiO_2–PdX–ZnY, more charge carriers were excited, separated and transferred to the surface of the photocatalyst than the TiO_2 samples modified with only Pd or Zn on the surface. When the electrons and holes migrate to the surface, the Zn and Pd surface species may act as reactive sites.

Because the energy level of O–Zn–Cl (−0.45 V, *vs.* NHE) locates above the reduction–oxidation potential of reaction (3) (−0.24 V, *vs.* NHE) and the level of O–Pd–O (1.7 V, *vs.* NHE) is below the potential of reaction (2) (+0.8V, *vs.* NHE) respectively, these photo-generated carriers on the surface would participate in the catalytic reaction upon reduction of CO_2 into CH_4. According to the discussion above, owing to the synergistic effect of O–Zn–Cl and O–Pd–O species on the TiO_2 surface, the visible response was improved significantly and charge carriers

were separated effectively. Moreover, the band structure for TiO_2–PdX–ZnY photocatalysts match preferably with the redox potential upon the photoreduction of CO_2 into CH_4, because of the energy levels of the O–Pd–O and O–Zn–Cl species. As a result, more photogenerated holes and electrons could be involved in the photocatalytic reduction, leading to a much higher photocatalytic activity for TiO_2–PdX–ZnY than for TiO_2–Pd and TiO_2–Zn.

Conclusions

A series of highly reactive photocatalysts, TiO_2–PdX–ZnY, were synthesized and exhibited significantly improved photo-reduction activity of CO_2 into CH_4. Because of the synergetic effect of surface O–Zn–Cl and O–Pd–O species, visible absorption was enhanced significantly and charge carriers were separated. Because the energy level of surface species is close to the redox potential of photo-reduction, more electrons and holes are enriched in the reactive sites (O–Zn–Cl and O–Pd–O surface species) and further participate in photo-reduction, leading to a remarkably improved photocatalytic activity for TiO_2–PdX–ZnY upon photoreduction of CO_2 into CH_4.

Conflicts of interest

There are no conflicts to declare.

Acknowledgements

This work was supported by the National Natural Science Foundation of China (no. 51372120) and China Postdoctoral Science Foundation (no. 2017M611149). We thank Prof. Yihong Ding from State Key Lab of Theoretical and Computational Chemistry, Jilin University for helping us to carry out the theoretical calculation.

Notes and references

1 S. N. Habisreutinger, L. Schmidt-Mende and J. K. Stolarczyk, *Angew. Chem., Int. Ed.*, 2013, **52**, 7372–7408.
2 K. F. Li, X. Q. An, K. H. Park, M. Khraisheh and J. W. Tang, *Catal. Today*, 2014, **224**, 3–12.
3 L. Yuan and Y. J. Xu, *Appl. Surf. Sci.*, 2015, **342**, 154–167.
4 O. Ola and M. M. Maroto-Valer, *J. Photochem. Photobiol., C*, 2015, **24**, 16–42.
5 S. Bai, W. Yin, L. Wang, Z. Li and Y. Xiong, *RSC Adv.*, 2016, **6**, S7446–S7463.
6 N. M. Dimitrijevic, B. K. Vijayan, O. G. Poluektov, T. Rajh, K. A. Gray, H. He and P. Zapol, *J. Am. Chem. Soc.*, 2011, **133**, 3964–3971.
7 Q. Liu, Y. Zhou, Z. Tian, X. Chen, J. Gao and Z. Zou, *J. Mater. Chem.*, 2012, **22**, 2033–2038.
8 S. Xie, Y. Wang, Q. Zhang, W. Fan, W. Deng and Y. Wang, *Chem. Commun.*, 2013, **49**, 2451–2453.
9 Y. Yan, Y. Yu, D. Wu, Y. Yang and Y. Cao, *Nanoscale*, 2015, **8**, 949–958.
10 Y. Yu, L. Guo, H. Cao, Y. Lv, E. Wang and Y. Cao, *Sep. Purif. Technol.*, 2015, **142**, 14–17.
11 E. Karamian and S. Sharifnia, *J. CO2 Util.*, 2016, **16**, 194–203.
12 K. Koci, L. Obalova and O. Solcova, *Chemical and Process Engineering-Inzynieria Chemiczna I Procesowa*, 2010, **31**, 395–407.
13 S. T. Seng, L. Zou and E. Hu, *Catal. Today*, 2008, **131**, 125–129.
14 K. Bhattacharyya, A. Danon, B. K. Vijayan, K. A. Gray, P. C. Stair and E. Weitz, *J. Phys. Chem. C*, 2013, **117**, 12661–12678.
15 V. V. Galvita, H. Poelman, C. Detavernier and G. B. Marin, *Appl. Catal., B*, 2015, **164**, 184–191.
16 C. Wang, R. L. Thompson, J. Baltrus and C. Matranga, *J. Phys. Lett.*, 2009, **1**, 48–53.
17 J. Low, B. Cheng and J. Yu, *Appl. Surf. Sci.*, 2017, **392**, 658–686.
18 L. Liu and Y. Li, *Aerosol Air Qual. Res.*, 2014, **14**, 453–469.
19 Y. Yan, Y. Yu, S. Huang, Y. Yang, X. Yang, S. Yin and Y. Cao, *J. Phys. Chem. C*, 2017, 1089–1098.
20 S. Yan, Y. Yu, Y. Gu, Y. Liu and Y. Cao, *Sep. Purif. Technol.*, 2016, **171**, 118–122.
21 Y. Yan, Y. Yu, C. Cao, S. Huang, Y. Yang, X. Yang and Y. Cao, *CrystEngComm*, 2016, **18**, 2956–2964.
22 M. Bowker, D. James, P. Stone, R. Bennett, N. Perkins, L. Millard, J. Greaves and A. Dickinson, *J. Catal.*, 2003, **217**, 427–433.
23 Y. Yu, J. Wang, W. Li, W. Zheng and Y. Cao, *CrystEngComm*, 2015, **17**, 5074–5080.
24 F. N. Sayed, O. Jayakumar, R. Sasikala, R. Kadam, S. R. Bharadwaj, L. Kienle, U. Schürmann, S. R. Kaps, R. Adelung and J. Mittal, *J. Phys. Chem. C*, 2012, **116**, 12462–12467.
25 A. T. Kuvarega, R. W. M. Krause and B. B. Mamba, *J. Phys. Chem. C*, 2011, **115**, 22110–22120.
26 Q. Li, Y. W. Li, P. Wu, R. Xie and J. K. Shang, *Adv. Mater.*, 2008, **20**, 3717–3723.
27 Q. Li, R. Xie, E. A. Mintz and J. K. Shang, *J. Am. Ceram. Soc.*, 2007, **90**, 3863–3868.
28 Y. Yu, E. Wang, J. Yuan and Y. Cao, *Appl. Surf. Sci.*, 2013, **273**, 638–644.
29 Y. Cao, T. He, L. Zhao, E. Wang, W. Yang and Y. Cao, *J. Phys. Chem. C*, 2009, **113**, 18121–18124.
30 Y. Cao, Y. Yu, P. Zhang, L. Zhang, T. He and Y. Cao, *Sep. Purif. Technol.*, 2013, **104**, 256–262.
31 J. Wang, Y. Yu, S. Li, L. Guo, E. Wang and Y. Cao, *J. Phys. Chem. C*, 2013, **117**, 27120–27126.
32 Y. Yu, T. He, L. Guo, Y. Yang, L. Guo, Y. Tang and Y. Cao, *Sci. Rep.*, 2015, **5**(9561), 1–6.
33 W. Li, D. Wu, Y. Yu, P. Zhang, J. Yuan, Y. Cao, Y. Cao and J. Xu, *Phys. E*, 2014, **58**, 118–123.
34 Y. Yu, Y. Gu, W. Zheng, Y. Ding and Y. Cao, *J. Phys. Chem. C*, 2015, **119**, 28190–28193.
35 Y. Cao, T. He, Y. Chen and Y. Cao, *J. Phys. Chem. C*, 2010, **114**, 3627–3633.

